Research Square

Preprints are preliminary reports that have not undergone peer review.
They should not be considered conclusive, used to inform clinical practice,
or referenced by the media as validated information.

Effect of n-Hexane Addition on the Structure and Morphology of CTAB-Templated Silica Nanoparticles

Zaineb O. Ettarhouni
University of Tripoli
Suad E. Abughrin
Libyan Authority for Scientific Research
Hager S. Elbeshti
University of Zawia
Salem A. Eljagmani
University of Zawia
Farahah S. ALamin
University of Tripoli
Khaled Edbey
University of Misurata
Ajaya Bhattarai
bkajaya@yahoo.com

Tribhuvan University

Research Article

Keywords: Silica nanoparticles, CTAB, TEOS, n-hexane, amorphous silica, XRD, SEM, TEM

Posted Date: November 25th, 2026

DOI: https://doi.org/10.21203/rs.3.rs-11757298/v1

License: This work is licensed under a Creative Commons Attribution 4.0 International License.
Read Full License

Additional Declarations: No competing interests reported.

Abstract

Silica nanoparticles were prepared by a cetyltrimethylammonium bromide (CTAB)-templated sol–gel route using tetraethyl orthosilicate (TEOS) and aqueous ammonia, with 0, 0.06, 0.1, 0.2, and 0.4 mL of n-hexane added to 20 mL of 0.055 mol L^{-1} CTAB solution, followed by calcination at 550°C. X-ray diffraction (XRD), scanning electron microscopy (SEM), and transmission electron microscopy (TEM) were used to examine the effect of the added oil. All XRD patterns show the broad halo of amorphous silica at 2θ = 22.1–22.9° (d = 3.89–4.02 Å), whose position is essentially independent of the hexane content. At 0.4 mL of n-hexane, the halo is narrower (FWHM 0.23° compared with 0.48–0.83° for the other samples), and an additional broad feature appears at 2θ = 12.8° (d = 6.92 Å). SEM shows spherical aggregates of about 690–1050 nm that become more densely packed and more strongly aggregated as the hexane content increases, and TEM shows nanoscale porous contrast in the aggregates. These results show that n-hexane modifies the aggregation and short-range structure of the CTAB-templated silica; confirmation of mesoporosity and of pore-size changes requires low-angle XRD or SAXS and nitrogen sorption, which were not available in this study.

1. Introduction

Mesoporous silica nanoparticles (MSNs) combine a high surface area with ordered pores that are typically 2–50 nm in diameter, which makes them attractive for drug delivery, catalysis, sensing and environmental remediation [1–3]. They are usually prepared by the sol–gel route, in which tetraethyl orthosilicate (TEOS) is hydrolysed and condensed around micelles of a structure-directing surfactant such as cetyltrimethylammonium bromide (CTAB) [4–6]. Because CTAB is amphiphilic, it assembles into micelles that template the pores and also influence the size and shape of the particles and the stability of the colloidal suspension [7–10].

The solvent and any co-solvent or oil in the synthesis mixture influence micelle size and packing, the rates of hydrolysis and condensation, and hence the pore structure and particle morphology. For example, the choice of alcohol (ethanol, methanol, isopropanol, butanol or tert-butanol) is reported to change the degree of pore order and the pore size through its polarity, evaporation rate and steric effects [11–14]. Ethanol is the most common solvent and generally gives well-ordered mesostructures, whereas more polar or more bulky alcohols tend to give less uniform pores [11].

Oils such as n-hexane are hydrophobic and can be solubilised in the hydrophobic core of CTAB micelles, where they swell the micelle and may change the packing of the surfactant and thereby the structure of the resulting silica. The effect of solvent content on the structural, morphological and nanostructural properties of CTAB/TEOS-derived silica is, however, still not fully understood [15–19].

The aim of this study was to examine how increasing amounts of n-hexane (0–0.4 mL in 20 mL of CTAB solution) change the structure and morphology of silica prepared with CTAB and TEOS, using XRD, SEM and TEM [20, 21].

2. Materials and Methods

2.1. Materials

CTAB (M.W. 364.4 g mol^{-1}, purity ≥ 98%, BDH, Poole, England), tetraethyl orthosilicate (TEOS; M.W. 208.33 g mol^{-1}, purity ≥ 98%, Gientham Life Sciences, UK), aqueous ammonia solution (25%, Merck, Germany) and n-hexane (M.W. 86.18 g mol^{-1}, purity 97%, Laboratory Supplies, Poole, England) were used as received. Deionized water was used throughout.

2.2. Synthesis procedure

CTAB (0.4 g, 1.10 mmol) was dissolved in 20 mL of deionized water to obtain a 0.055 mol L^{-1} solution. For the hexane-containing samples, n-hexane (0.06, 0.10, 0.20, or 0.40 mL) was first added to the CTAB solution. Subsequently, aqueous ammonia (25 wt%, 2.216 g) was added, followed by the addition of TEOS (98%, 0.008 mol, corresponding to approximately 1.667 g or 1.79 mL). The reaction mixture was continuously stirred at 500 rpm at room temperature for 1 h.

After stirring, the resulting white precipitate was collected by filtration, washed with approximately 70 mL of deionized water, and dried at 80–90°C for approximately 2 h. The dried samples were subsequently calcined in air at 550°C for 5 h, using a heating rate of 1 K min^{-1}, to remove the surfactant template.

To study the effect of the oil, n-hexane (0.06, 0.1, 0.2, and 0.4 mL) was added to the 0.055 mol L^{-1} CTAB solution, and the above procedure was followed. A hexane-free sample was prepared as a reference. The five samples are designated a–e (Table 1).

Table 1
Typical sample information and acronyms.

Oil content	Codes	Sample information
no oil	a	CTAB/ H_2O
0.06 mL	b	CTAB /H_2O/ (0.06 mL) hexane
0.1 mL	c	CTAB /H_2O/ (0.1 mL) hexane
0.2 mL	d	CTAB /H_2O/ (0.2 mL) hexane
0.4 mL	e	CTAB /H_2O/ (0.4 mL) hexane

2.3. Calcination

Calcination at 550°C removes the CTAB template and can also cause shrinkage and sintering of the silica network and fusion of small particles [22].

2.4. Instrumentations

X-ray diffraction (XRD) measurements were performed using a PANalytical X'Pert Pro diffractometer equipped with Cu Kα radiation (λ = 1.5406 Å). The diffraction patterns were recorded over a 2θ range of 5–70° to investigate the structural characteristics and crystallinity of the prepared silica nanoparticles (Table 2). SEM was performed on a Hitachi S-4300LV microscope with a Schottky field-emission gun. TEM was performed on a JEOL 2100 (LaB_6) high-resolution microscope equipped with a Gatan 2k × 2k digital camera and a HAADF (Z-contrast) detector.

Table 2
XRD data of samples a–e: position (2θ), interplanar spacing (d, from Eq. 1), and full width at half maximum (FWHM) of the broad halo; the additional feature of sample e is listed separately.

Sample	**n-Hexane (mL)**	**2θ (°) ± 0.02**	**d (Å) ± 0.004**	**FWHM (°) ± 0.030**
a	0	22.659	3.921	0.829
b	0.06	22.086	4.021	0.721
c	0.1	22.711	3.912	0.478
d	0.2	22.815	3.894	0.592
e	0.4	22.860	3.887	0.228
e (additional feature)	0.4	12.788	6.917	0.821

3. Results and Discussion

3.1. X-ray diffraction (XRD) study

XRD is the standard technique for characterizing the structure of these materials [23]. For a hexagonal mesophase, a reflection at a low angle (2θ < 8°) gives the pore-to-pore spacing; in amorphous silica, wide-angle patterns show only a broad halo. The interplanar spacing d was calculated from the peak position with Bragg's law (Eq. 1) [24].

$$n\,\lambda = 2\,d\,\sin\theta \quad (1)$$

where n is the diffraction order, d is the interplanar spacing, θ is the Bragg angle, and λ is the wavelength of the incident radiation (Cu Kα, λ = 1.5406 Å).

Amorphous silica has no periodic atomic planes, and its pattern consists of a broad halo at 2θ ≈ 22° (d ≈ 4 Å) that reflects the short-range Si–O–Si order [23, 24]. The d values obtained from this halo therefore describe short-range order and are not pore sizes.

Figure 1 shows the XRD patterns of samples a–e, which were prepared under identical conditions except for the amount of n-hexane. All patterns show the broad halo of amorphous silica, with its maximum at

2θ = 22.1–22.9° (Table 2). The position of the halo changes little with hexane content: d = 3.92, 4.02, 3.91, 3.89 and 3.89 Å for samples a–e, i.e., the variation (≤ 0.13 Å) is small compared with the width of the halo and is not significant without replicate measurements.

The FWHM of the halo decreased from 0.83° (a) and 0.72° (b) to 0.48° (c), 0.59° (d) and 0.23° (e), i.e., it was narrowest for the sample prepared with 0.4 mL of n-hexane (Table 2, Fig. 2). Since the material is amorphous, a narrower halo indicates a more uniform short-range Si–O–Si environment and not crystallinity or larger crystallites. Sample e also shows an additional broad feature at 2θ = 12.8° (d = 6.92 Å, FWHM 0.82°) that is absent from samples a–d.

A spacing of 6.9 Å is far too small to be the spacing of a mesophase (typically 2–5 nm), so this feature cannot be assigned to a second population of mesopores or to a bimodal pore-size distribution. Possible origins include an additional ordered domain, a minor crystalline impurity, or residual species from the template, which could not be distinguished with the present data. Its identification requires additional measurements (e.g., low-angle XRD or SAXS, FTIR or TGA of the calcined powder, and replicate syntheses).

The XRD data therefore show that n-hexane at 0.4 mL changes the short-range structure of the silica; they do not allow conclusions about pore size, pore-size distribution, or mesophase ordering. Pore characteristics could not be determined because low-angle XRD or SAXS patterns and nitrogen sorption isotherms were not available.

3.2. Microscopy observation

3.2.1. Transmission electron microscopy (TEM)

Figure 3 shows TEM images of samples a–e. The aggregates consist of nanoscale porous silica. Some regions show fringe-like contrast and others show a disordered, worm-like porous texture, and the annotated distances in the images are about 1–2 nm. The nature of these distances (pore-to-pore spacing, wall thickness, or fringe spacing), the number of measurements, and the sample–image assignment need to be specified, and a Fourier transform of the images would be needed to show whether the contrast is periodic. The observed texture is consistent with silica templated by surfactant micelles [25–29], but the images alone do not demonstrate a hexagonal (honeycomb) arrangement or a systematic effect of the hexane content.

Under the basic conditions used, the cationic head groups of CTAB interact electrostatically with negatively charged silicate species, and the micelles, whose formation is driven by the hydrophobic effect, act as templates for the condensation of TEOS-derived silica [20, 30]. The template is removed by calcination, which leaves the porous silica network [31, 32, 33].

3.2.2. Scanning electron microscopy (SEM)

SEM images of the samples are shown in Fig. S1 (supplementary information). All samples consist of spherical particles that form aggregates. Without n-hexane, the spheres are relatively well separated from each other. As the hexane content increases, the spheres are packed more closely and aggregate more strongly, and at 0.4 mL they form dense, interconnected clusters with a rougher surface [34–36].

The effect of hexane on the packing can be rationalized as follows, although it was not tested here. n-Hexane is solubilised in the hydrophobic core of the CTAB micelles and swells them, which can alter the CTAB packing, the rate of TEOS hydrolysis and condensation, and the interaction between growing silica particles, and thus their tendency to aggregate [31, 37].

The SEM images revealed aggregated silica particles with approximate dimensions in the range of 690–1050 nm. However, quantitative particle-size analysis was limited by particle overlap and the difficulty of distinguishing individual particle boundaries in the available images. Therefore, these dimensions should be considered approximate morphological observations rather than statistically representative particle-size distributions.

3.3. Comparison with the literature and limitations

Studies of silica aerogels, in which solvents are exchanged and removed during ambient-pressure drying, report that the solvent influences the pore microstructure and aggregation of the silica network [38, 39]. These systems differ from the present one, in which n-hexane acts as an oil in a surfactant-templated synthesis, so the comparison is only qualitative. The increase in particle aggregation with hexane content found here is in line with the general view that solvent composition affects the aggregation and morphology of silica particles [31, 35].

This study has several limitations. Nitrogen sorption (BET and BJH analysis) and low-angle XRD or SAXS were not available, so the surface area, pore size, and pore ordering of the samples could not be determined; values from the literature are therefore not given for comparison. The XRD interpretation is limited to the short-range structure of amorphous silica. The particle sizes and TEM spacings need statistics, and replicate measurements are not reported. Future work should combine low-angle XRD or SAXS with nitrogen sorption and with quantitative analysis of SEM and TEM images.

4. Conclusion

The addition of n-hexane to a CTAB/TEOS synthesis changed the structure and morphology of the resulting silica. All samples were amorphous, with a broad XRD halo at $2\theta \approx 22–23°$ whose position was independent of the hexane content. At 0.4 mL of n-hexane, the halo narrowed (FWHM 0.23°) and an additional broad feature appeared at $2\theta = 12.8°$ ($d = 6.92$ Å), which indicates a change in short-range structure but cannot be assigned to pores. SEM showed spherical particles whose packing and aggregation increased with the hexane content, and TEM showed nanoscale porous contrast without a clear dependence on hexane content. A bimodal pore-size distribution, a change in pore size, or an

increase in crystallinity could not be demonstrated by these data. The porosity of the materials should be confirmed by nitrogen sorption and low-angle XRD or SAXS.

Declarations

Conflicts of interest:

The authors reported no potential conflicts of interest.

Ethical approval:

Not Applicable.

Funding:

No specific funding was received.

Author Contribution

Zaineb O. Ettarhouni: Conceptualization, Data curation, Investigation, Writing – original draft. Suad E. Abughrin: Validation, Visualization, Writing – review & editing. Hager S. Elbeshti: Methodology, Project administration, Formal analysis. Salem A. Eljagmani: Validation, Funding acquisition, Writing – review & editing. Farahah S. ALamin: Methodology, Resources, Software. Ajaya Bhattarai and Khaled Edbey: Validation, Supervision, Writing – review & editing.

Acknowledgments:

One of the authors, Zaineb O. Ettarhouni, acknowledges the Department of Chemistry, Faculty of Science, University of Tripoli, Libya, for its laboratory facilities.

Data availability:

The data supporting this study will be made available by the authors on request.

References

1. Zhang W, Liu H, Qiu X, Zuo F, Wang B (2024) Mesoporous silica nanoparticles as a drug delivery mechanism. Open Life Sci 19:20220867. 10.1515/biol-2022-0867

2. Bose S, Sarkar N, Jo Y (2024) Natural medicine delivery from 3D-printed bone substitutes. J Control Release 365:848–875. 10.1016/j.jconrel.2023.09.025
3. Li B, Liao Y, Su X, Chen S, Wang X, Shen B, Yue P (2023) Powering mesoporous silica nanoparticles into bioactive nanoplatforms for antibacterial therapies: strategies and challenges. J Nanobiotechnol 21:325. 10.1186/s12951-023-02093-w
4. Abduraimova A, Molkenova A, Duisembekova A, Mulikova T, Kanayeva D, Atabaev TS (2021) Cetyltrimethylammonium bromide (CTAB)-loaded SiO2–Ag mesoporous nanocomposite as an efficient antibacterial agent. Nanomaterials 11:477. 10.3390/nano11020477
5. Kim MK, Ki DH, Na YG, Lee HS, Baek JS, Lee JY, Cho CW (2021) Optimization of mesoporous silica nanoparticles through statistical design of experiments and the application for the anticancer drug. Pharmaceutics 13:184. 10.3390/pharmaceutics13020184
6. Saman N, Othman NS, Chew LY, Setapar SHM, Mat H (2020) Cetyltrimethylammonium bromide-functionalized silica nanoparticles (MSN) synthesis using a combined sol-gel and adsorption steps with enhanced adsorption performance of oxytetracycline in aqueous solution. J Taiwan Inst Chem Eng 112:67–77. 10.1016/j.jtice.2020.07.008
7. Noureddine A, Maestas-Olguin A, Tang L, Corman-Hijar JI, Olewine M, Krawchuck JA, Tsala Ebode J, Edeh C, Dang C, Negrete OA, Watt J, Howard T, Coker EN, Guo J, Brinker CJ (2023) Future of Mesoporous Silica Nanoparticles in Nanomedicine: Protocol for Reproducible Synthesis, Characterization, Lipid Coating, and Loading of Therapeutics (Chemotherapeutic, Proteins, siRNA and mRNA). ACS Nano 17(17):16308–16325. https://doi.org/10.1021/acsnano.3c07621
8. Castillo RR, de la Torre L, García-Ochoa F, Ladero M, Vallet-Regí M (2020) Production of MCM-41 nanoparticles with control of particle size and structural properties: optimizing operational conditions during scale-up. Int J Mol Sci 21:7899
9. Li Q, Zhou Y (2023) Brief history, preparation method, and biological application of mesoporous silica molecular sieves: A narrative review. Molecules 28:2013
10. Han Y, Zhang L, Yang W (2024) Synthesis of mesoporous silica using the sol–gel approach: adjusting architecture and composition for novel applications. Nanomaterials 14:903
11. Narayan R, Nayak UY, Raichur AM, Garg S (2018) Mesoporous silica nanoparticles: A comprehensive review on synthesis and recent advances. Pharmaceutics 10:118. 10.3390/pharmaceutics10030118
12. Wu SH, Mou CY, Lin HP (2013) Synthesis of mesoporous silica nanoparticles. Chem Soc Rev 42:3862–3875. 10.1039/C3CS35405A
13. Li P, Li T, Ishiguro M, Su Y (2020) Comparison of same carbon chain length cationic and anionic surfactant adsorption on silica. Colloids Interfaces 4:34. 10.3390/colloids4030034
14. Qiao ZA, Zhang L, Guo M, Liu Y, Huo Q (2009) Synthesis of mesoporous silica nanoparticles via controlled hydrolysis and condensation of silicon alkoxide. Chem Mater 21:3823–3829. 10.1021/cm901335k
15. Mukhopadhyay S, Veroniaina H, Chimombe T, Han L, Zhenghong W, Xiaole Q (2019) Synthesis and compatibility evaluation of versatile mesoporous silica nanoparticles with red blood cells: an

overview. RSC Adv 9:35566–35578

16. Lin H-P, Mou C-Y (2002) Structural and Morphological Control of Cationic Surfactant-Templated Mesoporous Silica. Acc Chem Res 35(11):927–935. https://doi.org/10.1021/ar000074f
17. Ashour MM, Mabrouk M, Soliman IE, Beherei HH, Tohamy KM (2021) Mesoporous silica nanoparticles prepared by different methods for biomedical applications: Comparative study. IET Nanobiotechnol 15:291–300
18. Gottuso A, Armetta F, Cataldo A, Nardo VM, Parrino F, Saladino ML (2022) Functionalization of mesoporous silica nanoparticles through one-pot co-condensation in w/o emulsion. Microporous Mesoporous Mater 335:111833
19. Qu H, Yang L, Yu J, Dong T, Rong M, Zhang J, Liu H (2017) A redox-responsive controlled release system using mesoporous silica nanoparticles capped with Au nanoparticles. RSC Adv 7:35704–35710
20. Baig N, Kammakakam I, Falath W (2021) Nanomaterials: A review of synthesis methods, properties, recent progress, and challenges. Mater Adv 2:1821–1871
21. Pal N, Lee JH, Cho EB (2020) Recent trends in morphology-controlled synthesis and application of mesoporous silica nanoparticles. Nanomaterials 10:2122. 10.3390/nano10112122
22. Kumar R, Chen HT, Escoto JL, Lin VSY, Pruski M (2006) Template removal and thermal stability of organically functionalized mesoporous silica nanoparticles. Chem Mater 18:4319–4327
23. Chircov C, Spoială A, Păun C, Crăciun L, Ficai D, Ficai A, Turculeț ȘC (2020) Mesoporous silica platforms with potential applications in release and adsorption of active agents, Molecules 25 3814.10.3390/molecules25043814
24. Bunaciu AA, Udriștioiu EG, Aboul-Enein HY (2015) X-ray diffraction: instrumentation and applications. Crit Rev Anal Chem 45:289–299
25. Lodha A, Lodha M, Patel A, Chaudhuri J, Dalal J, Edwards M, Douroumis D (2012) Synthesis of mesoporous silica nanoparticles and drug loading of poorly water-soluble drug cyclosporin A. J Pharm Bioallied Sci 4:S92–S94
26. Vitale F, Saladino ML, Armetta F, Presentato A, Alduina R, Mercadante A, La Parola V, Giacalone F (2022) New Biocides Based on Imidazolinium-Functionalised Hybrid Mesoporous Silica Nanoparticles. Microporous Mesoporous Mater 343:112142. https://doi.org/10.1016/j.micromeso.2022.112142
27. Gao B, Hu M, Wang J, Xu C, Chen Z, Fan H, Ding H (2020) Spatial interpolation of marine environment data using P-MSN. Int J Geogr Inf Sci 34:577–603
28. Saravanan M, Sudalai S, Dharaneesh AB, Prahaaladhan V, Srinivasan G, Arumugam A (2023) An extensive review on mesoporous silica from inexpensive resources: Properties, synthesis, and application toward modern technologies. J Sol-Gel Sci Technol 105:1–29
29. Deshmukh PK, Lakade SH, Jaiswal UR, Harde MT, More MP (2022) One-step synthesis approach of mesoporous silica packed with graphene oxide nanosheet: Characterisation and drug release aspects. Mater Technol 37:1677–1690

30. Li H, Chen X, Shen D, Wu F, Pleixats R, Pan J (2021) Functionalized silica nanoparticles: classification, synthetic approaches and recent advances in adsorption applications. Nanoscale 13:15998–16016
31. Guerra FD, Attia MF, Whitehead DC, Alexis F (2018) Nanatechnol Environ Remediation: Mater Appl Molecules 23(7):1760. https://doi.org/10.3390/molecules23071760
32. Jacobson AT, Chen C, Dewey JC, Copeland GC, Allen WT, Richards B, Martin TP (2022) Effect of nanoconfinement and pore geometry on point of zero charge in synthesized mesoporous siliceous materials. JCIS Open 8:100069. 10.1016/j.jciso.2022.100069
33. Tarn D, Ashley CE, Xue MI, Carnes EC, Zink JI, Brinker CJ (2013) Mesoporous silica nanoparticle nanocarriers: biofunctionality and biocompatibility. Acc Chem Res 46:792–801. 10.1021/ar3000986
34. Xu C, Lei C, Wang Y, Yu C (2022) Dendritic mesoporous nanoparticles: structure, synthesis and properties. Angew Chem Int Ed 61:e202112752. 10.1002/anie.202112752
35. Luo L, Liang Y, Erichsen ES, Anwander R (2018) Hierarchical mesoporous organosilica–silica core–shell nanoparticles capable of controlled fungicide release. Chem Eur J 24:7200–7209
36. Croissant JG, Fatieiev Y, Khashab NM (2017) Degradability and clearance of silicon, organosilica, silsesquioxane, silica mixed oxide, and mesoporous silica nanoparticles. Adv Mater 29:1604634. 10.1002/adma.201604634
37. Yang Y, Hao J, Cui J (2024) Engineering of hierarchical mesoporous silica nanoparticles via control over surfactant nanoarchitectonics for biological applications. Curr Opin Colloid Interface Sci. 101819
38. Zemke F, Scoppola E, Simon U, Bekheet MF, Wagermaier W, Gurlo A (2022) Springback effect and structural features during the drying of silica aerogels tracked by in-situ synchrotron X-ray scattering. Sci Rep 12:7537. 10.1038/s41598-022-11127-6
39. Duan L et al (2023) Enhancing the structural integrity of silica aerogels by modulating the pore microstructure and crystallinity during ambient pressure drying. J Non-Cryst Solids 608:121501

Figures

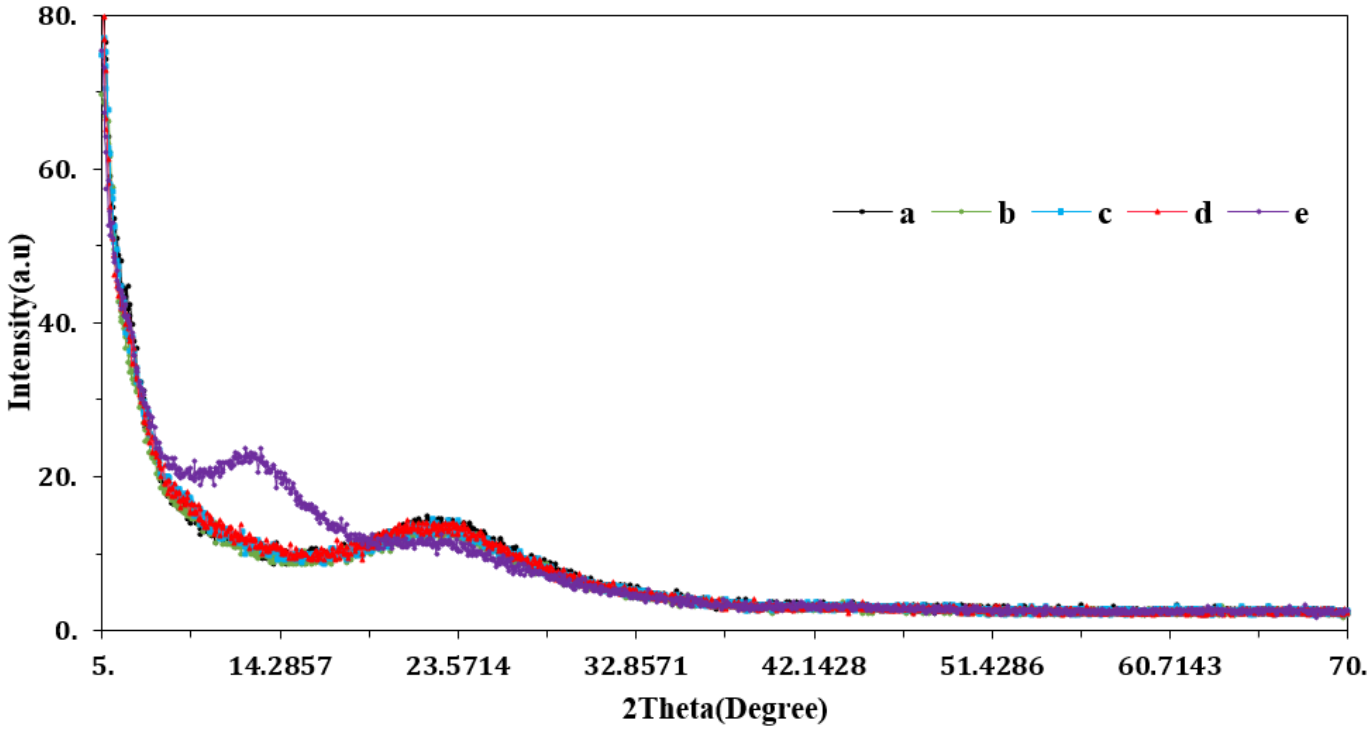


Figure 1

XRD patterns of mesoporous silica nanoparticles with variations in n-hexane. a) no hexane (black line), b) 0.06 mL n-hexane (green line), c) 0.1 mL n-hexane (blue line), d) 0.2 mL n-hexane (red line), e) 0.4 mL n-hexane (purple line).

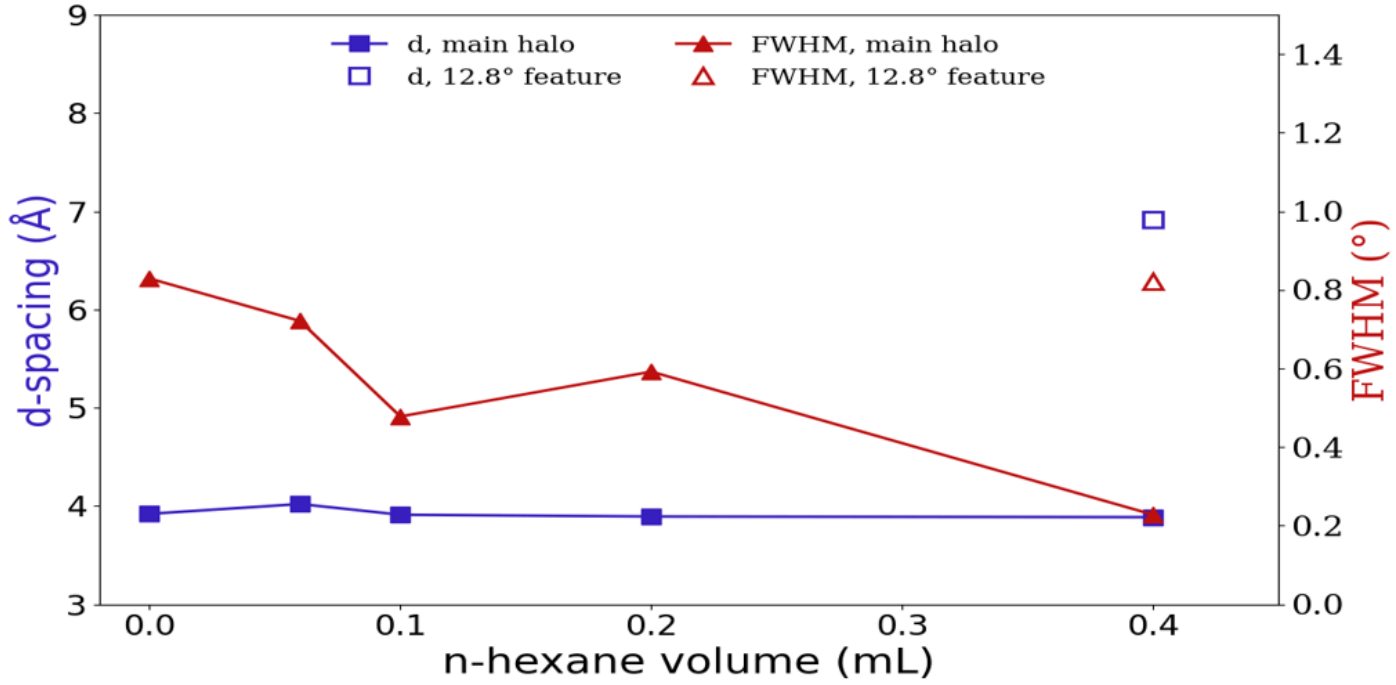


Figure 2

Interplanar spacing d (squares, left axis) and FWHM (triangles, right axis) of the main XRD halo as a function of the n-hexane volume. Open symbols: additional feature at 2θ = 12.8° (sample e).

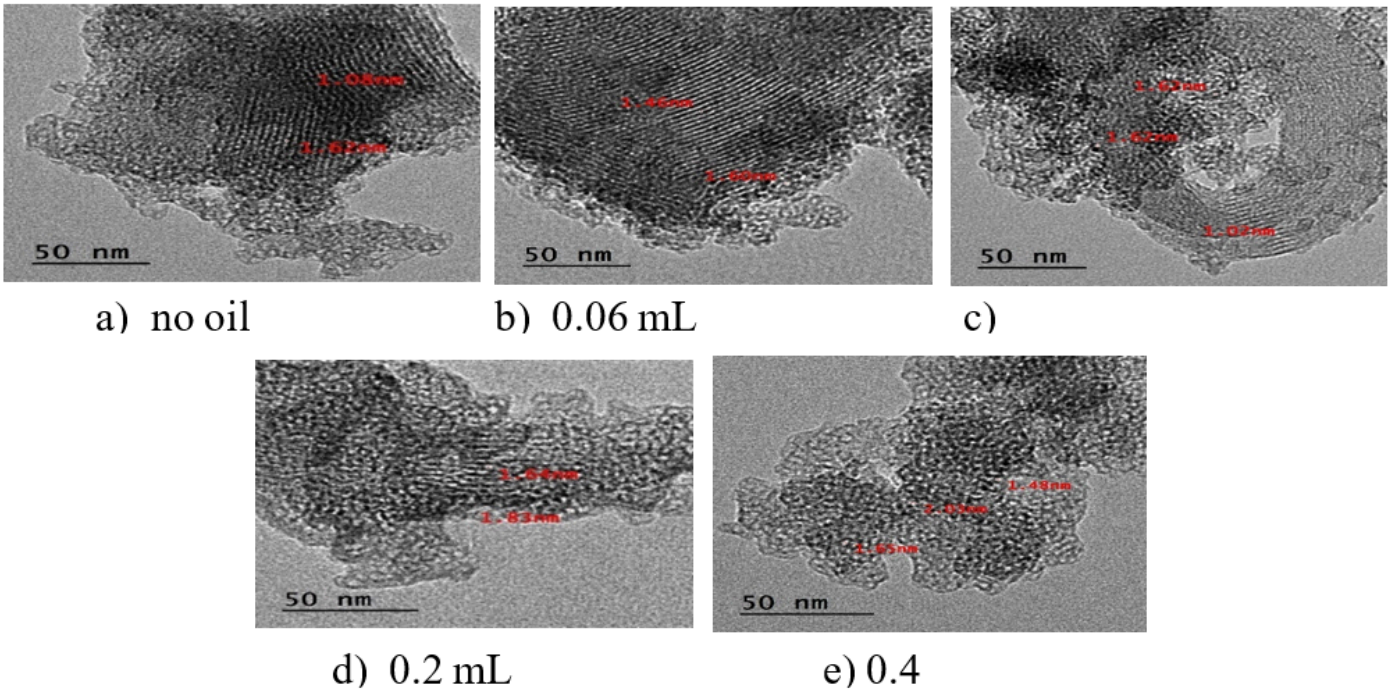


Figure 3

TEM images of synthesized nanoporous silica: a) no oil, b) 0.06 mL, c) 0.1 mL, d) 0.2 mL, and e) 0.4 mL.

Supplementary Files

This is a list of supplementary files associated with this preprint. Click to download.

- Supplementaryfile16Nov2026.docx